# SPECT Quantification of Benzodiazepine Receptor Concentration Using a Dual-Ligand Approach

Philippe Millet[1], Christophe Graf[1], Marcelle Moulin[2], and Vicente Ibáñez[1]

[1]Psychiatric Neuroimaging Unit, Division of Neuropsychiatry, Department of Psychiatry, University Hospitals of Geneva, Geneva, Switzerland; and [2]INSERM, E340, Grenoble, France

The distribution of benzodiazepine receptors in the human brain has been widely studied with SPECT using $^{123}$I-iomazenil and semiquantitative approaches, but these methods do not allow quantification of the total receptor site concentration available for binding ($B'_{max}$) and of the apparent equilibrium dissociation constant ($K_d/V_R$). One of the major obstacles to full quantitative studies is that pharmacologic effects preclude the administration to humans of the high doses of iomazenil required to displace the labeled ligand from the receptors. In this study, we applied a dual-ligand protocol using the unlabeled ligand flumazenil, which lacks pharmacologic effects, to quantify all binding parameters of the benzodiazepine receptor–$^{123}$I-iomazenil interactions. **Methods:** $^{123}$I-Iomazenil SPECT and MRI were acquired in 8 healthy volunteers, one of whom had participated in a $^{11}$C-flumazenil PET experiment. The experimental protocol consisted of injections of $^{123}$I-iomazenil and/or unlabeled flumazenil. We developed a kinetic model to integrate the different pharmacokinetics of these 2 ligands. To simplify the model, we assumed linear relationships between iomazenil and flumazenil parameters and adjusted them using a coupled fitting procedure. The resulting constrained 5-parameter model was then used to quantify the biologic parameters. **Results:** Across regions, we obtained $B'_{max}$ values ranging from 7 to 69 pmol/mL and $K_dV_R$ values for IMZ from 2.3 to 3.7 pmol/mL. There was a close correlation in the $B'_{max}$ values calculated in the same volunteer using $^{123}$I-iomazenil SPECT and $^{11}$C-flumazenil PET. **Conclusion:** The dual-ligand approach can be used to quantify all model parameters with acceptable SEs. This work demonstrates a theoretic framework and initial application of SPECT to quantify binding parameters.

**Key Words:** SPECT; benzodiazepine; iomazenil; mathematic modeling

**B**enzodiazepine receptors have been implicated in the pathophysiology of several neurologic and psychiatric disorders (*1–3*). In humans, the distribution of these

receptors has been mainly studied using PET and $^{11}$C-flumazenil ($^{11}$C-FMZ) (*4–6*) as well as using SPECT and $^{123}$I-iomazenil ($^{123}$I-IMZ) (*4–9*).

Because of the increasing use of PET and SPECT for routine clinical diagnosis, quantitative and semiquantitative methods have been developed using $^{11}$C-FMZ and $^{123}$I-IMZ. PET has been used mainly for quantitative studies with multiinjection protocols (*10,11*). With an appropriate mathematic model, it is possible to extract from PET kinetic data absolute values of biologic parameters, including the total receptor site concentration available for binding ($B'_{max}$) and ligand affinity ($1/K_d$) ($K_d$ is the equilibrium dissociation constant) (*10,12*). In contrast, although more accessible than PET, SPECT provides little information about $B'_{max}$ and $K_d$ for the $^{123}$I-IMZ radioligand. The absolute quantification of benzodiazepine receptors using $^{123}$I-IMZ has been hampered by lower sensitivity of the scanners for SPECT than those for PET. Consequently, SPECT studies have been restricted to semiquantitative approaches that typically calculate only an index of receptor concentration, such as the binding potential (BP) or the distribution volume (DV) (*7,8,13–15*). However, these simplified approaches are based on several assumptions, which should be verified for each radioligand before any routine use. Indeed, the ability to derive accurate receptor-binding information from the DV or BP largely depends on the pharmacokinetic properties of the radiotracer (*13*). A full quantitative approach is essential to validate these underlying assumptions and, by comparing the indices of binding parameters with the $B'_{max}$, it evaluates the efficiency and robustness of these indices (*14,16*).

The emergence of a new generation of SPECT scanners with better resolution and sensitivity has allowed optimization of experimental protocols for estimating $B'_{max}$ and $K_d$. To do this, the radioligand must be injected at different specific activities along with large doses of unlabeled ligand. However, IMZ is a partial inverse agonist with several pharmacologic effects and, therefore, cannot be administered to humans at high doses (*17*).

In the present work, we used a full quantitative approach with SPECT to study the interaction between benzodiazepine

receptors and ^{123}I-IMZ. This approach was based on the multiinjection protocol defined by Delforge et al. (10) for PET studies. Because FMZ is an antagonist without pharmacologic effects when injected at high doses, we used it instead of IMZ as the unlabeled ligand (18). In addition, we developed a kinetic model to integrate the different affinities of the unlabeled and labeled ligands. We show that this dual-ligand approach allows the quantification of receptor concentration and ligand affinity from SPECT data.

## MATERIALS AND METHODS

### Subjects

Eight healthy volunteers (mean ± SD, 27.1 ± 7.3 y; range, 22-46 y; 7 males, 1 female) with no history of neurologic or psychiatric diseases participated in this study. Images from SPECT and MRI were acquired for all volunteers. Data from 1 of these volunteers who had already participated in a previous study (14) were used for a direct PET and SPECT comparison of $B'_{max}$. All volunteers gave informed consent before scanning, and the studies were approved by the Research Ethics Committee of Geneva Hospital.

### SPECT Experiments

During the scans, the subjects were lying with the head positioned in a head holder so that the transaxial slices were parallel to the orbitomeatal line. Scans were acquired with a Toshiba GCA-9300A/HG triple-head SPECT system in continuous rotation mode using a superhigh-resolution fanbeam collimator (19,20). Based on a radius of 132 mm, the tomographic spatial resolution at the center was 7.8-mm full width at half maximum with the superhigh-resolution fanbeam collimator. Raw data were reconstructed by filtered backprojection (Shepp and Logan filter) and corrected using the triple-energy window scatter correction method presented by Ogawa et al. (21). The images were corrected for attenuation using the Chang filtered method. The attenuation correction coefficient, μ, was set at 0.150 cm$^{-1}$, assuming uniform attenuation equal to that of 160-keV γ-ray water within an ellipse drawn around the transaxial plane (22). Images were displayed on a 128 × 128 × 46 matrix (pixel size = 1.72 ×

1.72 × 6.88 mm). Activities in cpm/mL were then converted to μCi/mL using a calibration procedure (14). Briefly, the phantom used for calibration was an ^{123}I distributed source (50 MBq) of 6-cm diameter acquired for 15 min and reconstructed with the same protocol used in this study. The average cpm/mL was measured with a large region of interest (ROI) positioned in the phantom image. One sample (1 mL) of the phantom solution was measured with the γ-counting system to determine the calibration factor between SPECT and γ-counting system measurements.

The multiinjection protocol requires injection of a labeled ligand, displacement by injection of the unlabeled ligand, and coinjection of labeled and unlabeled ligand. To ascertain if a low tracer signal level at the time of displacement can influence the estimation of some of the kinetic parameters, we switched the order of the displacement and the coinjection in half of the volunteers. Therefore, SPECT scans were performed using one of the following 2 protocols: protocol 1 included ^{123}I-IMZ injection at the start time (T0), displacement by injection with unlabeled FMZ at T0 + 70 min, and coinjection of ^{123}I-IMZ and unlabeled FMZ at T0 + 110 min; protocol 2 included ^{123}I-IMZ injection at T0, coinjection of ^{123}I-IMZ and unlabeled FMZ at T0 + 70 min, and displacement by injection with unlabeled FMZ at T0 + 110 min.

At the scan start time, approximately 74 MBq of ^{123}I-IMZ were injected intravenously. The displacement procedure consisted of injection of 0.02 mg/kg of FMZ, and the coinjection procedure used a mixture of 74 MBq ^{123}I-IMZ and 0.02 mg/kg FMZ. All injections were administered with a constant volume (30 mL) over a 1-min period using an infusion pump. Details of the injected doses and specific activities are listed in Table 1. A set of 80 sequential 2-min SPECT scans was obtained over 160 min.

### PET Experiment

Details of the PET experiment, performed on 1 healthy volunteer with a whole-body scanner (Advance; GE Healthcare), have been previously reported (14).

In brief, the brain transaxial images were reconstructed using a filtered backprojection (128 × 128 matrix; 35 slices; 2.34 × 2.34 × 4.25 mm voxel size). A 10-min transmission scan was obtained to correct for photon tissue attenuation. The data were also corrected for decay.

**TABLE 1**
Numeric Values of PET and SPECT Protocol Parameters Corresponding to 8 Experiments

| Subject no. | Modality/protocol | Duration (min) | Injection 1 (T = 0 min) | | Injection 2 | | | Injection 3 | | |
| | | | SA* (GBq/μmol) | $J_1^*$ (mg) | Time (min) | $J_2^*$ (mg) | $J_2$ (mg) | Time (min) | $J_3^*$ (mg) | $J_3$ (mg) |
|---|---|---|---|---|---|---|---|---|---|---|
| 1 | SPECT/1 | 160 | 156.81 | 0.133 | 70 | — | 0.73 | 110 | 0.140 | 1.46 |
| 2 | SPECT/1 | 160 | 156.18 | 0.138 | 70 | — | 1.28 | 110 | 0.154 | 1.28 |
| 3 | SPECT/1 | 160 | 95.68 | 0.212 | 70 | — | 1.34 | 110 | 0.248 | 1.34 |
| 4 | SPECT/1 | 160 | 91.69 | 0.219 | 70 | — | 2.00 | 110 | 0.322 | 2.00 |
| 5 | SPECT/2 | 160 | 68.78 | 0.335 | 70 | 0.381 | 1.64 | 110 | — | 1.64 |
| 6 | SPECT/2 | 160 | 113.18 | 0.201 | 70 | 0.229 | 1.44 | 110 | — | 1.44 |
| 7 | SPECT/2 | 160 | 107.41 | 0.218 | 70 | 0.238 | 1.44 | 110 | — | 1.44 |
| 8 | SPECT/2 | 160 | 100.86 | 0.232 | 70 | 0.252 | 1.54 | 110 | — | 1.54 |
| 7 | PET | 104 | 109.96 | 0.467 | 30 | — | 0.70 | 60 | 3.490 | 1.40 |

*Specific activity at beginning of experiment.
Doses $J_i^*$ and $J_i$ correspond, respectively, to labeled and unlabeled ligand doses injected during the $i$th injection.

The PET protocol consisted of 3 intravenous injections: injection of the tracer (148 MBq of $^{11}$C-FMZ) at T0, injection of unlabeled 0.01 mg/kg FMZ at T0 + 30 min, and coinjection of labeled (148 MBq) and unlabeled (0.02 mg/kg) FMZ at T0 + 60 min (10). All injections were administered over a 1-min period using an infusion pump. Details of injected doses and specific activities are listed in Table 1. A set of 48 sequential PET scans of increasing duration after each injection of labeled FMZ was obtained over a 104-min period (14).

## Analysis of Arterial Plasma

To assess the labeled input function of radiotracers, $C_p^*(t)$, an arterial catheter was inserted into the radial artery under local anesthesia and after establishing the presence of satisfactory collateral circulation. Fifty-one 3-mL arterial whole blood samples were manually withdrawn during the SPECT experiments (57 for the PET experiment): 1 sample was taken every 15 s during the first 4 min, after which samples were taken following an additional 30 s and 1, 2, and 5 min. The $^{123}$I-IMZ and $^{11}$C-FMZ metabolites were measured using 45 and 37 blood samples, respectively. Metabolites were extracted using a chloroform separation procedure (23–25) in which the radioactivity in the chloroform layer represents the amount of unchanged radioligand remaining in the plasma (25). After a rapid centrifugation of the blood (5,000$g$ for 5 min at 4°C), the $^{123}$I and $^{11}$C radioactivity in the plasma was measured using a γ-counting system (Packard Cobra II; Perkin-Elmer) and corrected for physical decay.

For quantitative purposes, $C_p^*(t)$ was fitted using 3- and 1-exponent models for $^{123}$I-IMZ and $^{11}$C-FMZ, respectively. $^{123}$I-IMZ metabolism is faster than that of $^{11}$C-FMZ. Therefore, the relative clearance of the free $^{123}$I-IMZ parent compound is better described by a 3-exponent model (8,10). Measurements in units of cpm/mL were converted into units of MBq/mL using a calibration factor that had been obtained before each experiment with an appropriate calibrated phantom (14).

## Compartmental Models

Figure 1 shows the appropriate 3-compartment model used to fit the SPECT data. In this model, the kinetics of the unlabeled ligand affected the local concentration of free receptor sites and

must therefore be considered. Moreover, the kinetics of the labeled $^{123}$I-IMZ and the unlabeled FMZ ligand are different. Therefore, the model includes competition of the labeled $^{123}$I-IMZ and the unlabeled FMZ for the same receptors. The 2 ligands have their own individual parameters except for the total receptor site concentration available for binding $B_{max}'$, which is common to both ligands. $C_p^*(t)$ and $C_p(t)$ are the input functions of the model, and they correspond to the plasma concentration of the unchanged labeled ($^{123}$I-IMZ) and unlabeled (FMZ) ligands, respectively. Parameter identification and simulations of labeled and unlabeled ligand kinetics were performed using the equation system corresponding to the model shown in Figure 1.

The labeled IMZ kinetics are described by the following relationships:

$$\frac{dM_{f+ns}^*(t)}{dt} = K_{1\text{-IMZ}}C_p^*(t) - k_{2\text{-IMZ}}'M_{f+ns}^*(t) - \frac{k_{on\text{-IMZ}}}{V_{R\text{-IMZ}}}$$
$$\times [B_{max}' - M_s^*(t) - M_s(t)]M_{f+ns}^*(t) + k_{off\text{-IMZ}}M_s^*(t),$$
$$\text{Eq. 1}$$

$$\frac{dM_s^*(t)}{dt} = \frac{k_{on\text{-IMZ}}}{V_{R\text{-IMZ}}}[B_{max}' - M_s^*(t) - M_s(t)]M_{f+ns}^*(t) - k_{off\text{-IMZ}}M_s^*(t),$$
$$\text{Eq. 2}$$

and the unlabeled FMZ kinetics are described by:

$$\frac{dM_{f+ns}(t)}{dt} = K_{1\text{-FMZ}}C_p(t) - k_{2\text{-FMZ}}'M_{f+ns}(t) - \frac{k_{on\text{-FMZ}}}{V_{R\text{-FMZ}}}$$
$$\times [B_{max}' - M_s^*(t) - M_s(t)]M_{f+ns}(t) + k_{off\text{-FMZ}}M_s(t),$$
$$\text{Eq. 3}$$

$$\frac{dM_s(t)}{dt} = \frac{k_{on\text{-FMZ}}}{V_{R\text{-FMZ}}}[B_{max}' - M_s^*(t) - M_s(t)]M_{f+ns}(t) - k_{off\text{-FMZ}}M_s(t),$$
$$\text{Eq. 4}$$

where $B_{max}'$, $K_{1\text{-IMZ}}$, $k_{2\text{-IMZ}}'$, $k_{on\text{-IMZ}}/V_{R\text{-IMZ}}$, $k_{off\text{-IMZ}}$, $K_{1\text{-FMZ}}$, $k_{2\text{-FMZ}}'$, $k_{on\text{-FMZ}}/V_{R\text{-FMZ}}$, $k_{off\text{-FMZ}}$, are the unknown parameters.
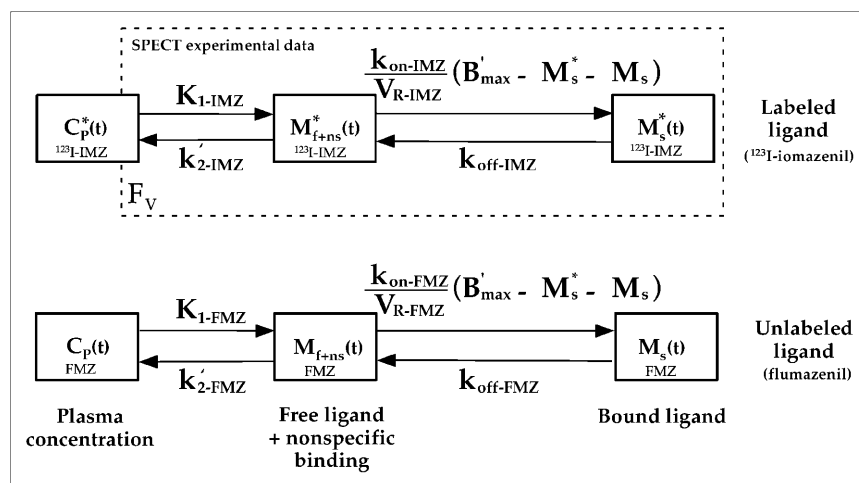


**FIGURE 1.** Three-compartment model used to fit SPECT data. This model contains 2 components for labeled and unlabeled ligands with individual parameters for IMZ and FMZ. Compartments $C_p^*(t)$ and $C_p(t)$ represent unchanged plasma $^{123}$I-IMZ and FMZ, respectively; $M_{f+ns}(t)$ represents free and nonspecifically bound ligand, and $M_s(t)$ represents specifically bound ligand. Parameters $K_1$ and $k_2'$ are associated with exchanges between plasma and free/nonspecifically bound ligand compartment. $B_{max}'$ represents concentration of receptors available for binding and is defined as the common parameter of the model; $k_{on}$ and $k_{off}$ are association and dissociation rate constants, respectively; and $V_R$ is volume of the reaction, which accounts for tissue inhomogeneity (26). Consequently, only the apparent equilibrium dissociation constant, $K_dV_R$, can be estimated. $K_d$ is equilibrium dissociation constant, defined as the ratio of $k_{off}$ to $k_{on}$. Parameter $F_V$ represents the fraction of blood present in tissue volume and was fixed at 0.04 (13,27,28).

The parameters $K_1$ and $k'_2$ are associated with the exchanges between the plasma and the free/nonspecifically bound ligand compartment. The $k_{on}$ and $k_{off}$ parameters are the association and dissociation rate constants, respectively; and $V_R$ is the volume of the reaction, which accounts for tissue inhomogeneity (26). Consequently, only the apparent equilibrium dissociation constant, $K_d V_R$, can be estimated. $K_d$ is the equilibrium dissociation constant, defined as the ratio of $k_{off}$ to $k_{on}$. The parameter $F_V$ represents the fraction of blood present in the tissue volume and was fixed at 0.04 (13,27,28). $M_{f+ns}(t)$ represents the quantity of the free and nonspecifically bound ligand; and $M_s(t)$ represents the quantity of specifically bound ligand. The $M^*(t)$ and $M(t)$ refer to labeled and unlabeled ligand, respectively.

The SPECT experimental data, denoted by $M_T^*(t_i)$, collected between times $t_{i-1}$ and $t_i$, are given by the following integral relationship:

$$M_T^*(t_i) = \frac{1}{(t_i - t_{i-1})} \int_{t_{i-1}}^{t_i} \left[ M_{f+ns}^*(t) + M_s^*(t) + F_V C_p^*(t) \right]. \quad \text{Eq. 5}$$

From the estimated model parameters, the distribution volume can be calculated using the following equation (13):

$$DV_T = DV_{f+ns} + DV_s = \frac{K_1}{k'_2} + \frac{K_1 k'_3}{k'_2 k_4} = \frac{K_1}{k'_2}$$
$$\times \left( 1 + \frac{(k_{on}/V_R)B'_{max}}{k_{off}} \right) = \frac{K_1}{k'_2} \left( 1 + \frac{B'_{max}}{K_d V_R} \right). \quad \text{Eq. 6}$$

Using the first 70 min of the SPECT protocol (data corresponding to the first injection), $K_1$ and $k''_2$ can be estimated with a 1 tissue-compartment model (13) from which the $DV_T''$ parameters are calculated:

$$DV_T'' = \frac{K_1}{k''_2}. \quad \text{Eq. 7}$$

## Simplification of Model Parameters

The model defined in Figure 1 involves 9 unknown parameters ($B'_{max}$, $K_{1\text{-IMZ}}$, $k'_{2\text{-IMZ}}$, $k_{on\text{-IMZ}}/V_{R\text{-IMZ}}$, $k_{off\text{-IMZ}}$, $K_{1\text{-FMZ}}$, $k'_{2\text{-FMZ}}$, $k_{on\text{-FMZ}}/V_{R\text{-FMZ}}$, $k_{off\text{-FMZ}}$). All of these parameters cannot be estimated together using PET or SPECT data. Therefore, we have to simplify the model.

If we consider the following relationship deduced from the Renkin–Crone equation (29):

$$K_1 = F E = F(1 - \exp(-PS/F)), \quad \text{Eq. 8}$$

where extraction (E) is related to flow (F), and to the product of permeability (P) and capillary surface area (S):

$$K_{1\text{-IMZ}} = F E_{IMZ}, \quad \text{Eq. 9}$$

and

$$K_{1\text{-FMZ}} = F E_{FMZ}, \quad \text{Eq. 10}$$

and the distribution volume for each tracer:

$$DV_{f+ns\text{-IMZ}} = \frac{K_{1\text{-IMZ}}}{k'_{2\text{-IMZ}}}, \quad \text{Eq. 11}$$

and

$$DV_{f+ns\text{-FMZ}} = \frac{K_{1\text{-FMZ}}}{k'_{2\text{-FMZ}}}, \quad \text{Eq. 12}$$

we can deduce that:

$$K_{1\text{-FMZ}} = A \, K_{1\text{-IMZ}}, \quad \text{Eq. 13}$$

where $A = E_{FMZ}/E_{IMZ}$ and that:

$$k'_{2\text{-FMZ}} = B \, k'_{2\text{-IMZ}}, \quad \text{Eq. 14}$$

where $B = A\, DV_{f+ns\text{-IMZ}}/DV_{f+ns\text{-FMZ}}$. Because only the permeability (P) of each ligand is different, we assume that A is a constant. If we consider the following definitions:

$$BP_{IMZ} = \frac{k_{on\text{-IMZ}} B'_{max}}{k_{off\text{-IMZ}}}, \quad \text{Eq. 15}$$

and

$$BP_{FMZ} = \frac{k_{on\text{-FMZ}} B'_{max}}{k_{off\text{-FMZ}}}, \quad \text{Eq. 16}$$

we can deduce that:

$$k_{on\text{-FMZ}} = C \, k_{on\text{-IMZ}}, \quad \text{Eq. 17}$$

where

$$C = \frac{BP_{FMZ}}{BP_{IMZ}} D \quad \text{and} \quad D = \frac{k_{off\text{-FMZ}}}{k_{off\text{-IMZ}}}. \quad \text{Eq. 18}$$

We used Equations 13, 14, 17, and 18 to define A, B, C, and D parameters, which are expected to be constant in the whole brain. If the A, B, C, and D values are known, the resulting constrained model requires the estimation of only 5 parameters.

Therefore, a coupled fit is first used to correctly estimate for each volunteer the A, B, C, and D IMZ and FMZ common parameters among several ROIs. Briefly, we obtained for each volunteer the time−concentration curves from 8 ROIs (radius = 5 mm) that are to be included in coupled fitting. Using these dynamic data and the constrained model, the coupled fit of the 8 ROIs, finds a separate $K_{1\text{-IMZ}}$, $k'_{2\text{-IMZ}}$, $k_{on\text{-IMZ}}/V_{R\text{-IMZ}}$, $k_{off\text{-IMZ}}$, and $B'_{max}$ for each curve, but delivers the A, B, C, and D common to the 8 regions. This method improves the identification of common parameters (30,31).

Finally, in a second fit, these common parameters were used as fixed constants in the model that was applied to the ROIs described in the data analysis, to estimate the kinetic parameters: $K_{1\text{-IMZ}}$, $k'_{2\text{-IMZ}}$, $k_{on\text{-IMZ}}/V_{R\text{-IMZ}}$, $k_{off\text{-IMZ}}$, and $B'_{max}$.

## Input Functions of Model

To solve the equation system corresponding to the model shown in Figure 1, the time course of $C_P(t)$ (unlabeled ligand) must be

known. When using the same ligand for the labeled and unlabeled injections, as is the case for the PET and FMZ experiments, it is possible to calculate $C_P(t)$ from the $C_P^*(t)$ measurements, using the following equation: $C_P(t) = (J/J^*)C_P^*(t - t_D)$, where J and $J^*$ represent the labeled and unlabeled injected doses, and $t_D$ is the delay between labeled and unlabeled injections (32). In the case of our SPECT experiments, the use of different ligands for labeled ($^{123}$I-IMZ) and unlabeled (FMZ) injections precludes the application of this relationship. Therefore, to obtain the time course for unlabeled FMZ from $^{123}$I-IMZ, we calculated the relationship between the plasma kinetics for $^{11}$C-FMZ and $^{123}$I-IMZ using blood data from a previous study (14). In this former study, we had obtained arterial input functions in 7 volunteers who underwent both $^{11}$C-FMZ PET and $^{123}$I-IMZ SPECT scans. The averaged $^{11}$C-FMZ and $^{123}$I-IMZ plasma time–concentration curves obtained from this previous study are shown in Figure 2. $^{123}$I-IMZ metabolism was faster than that of $^{11}$C-FMZ, which leads to a different whole plasma time course. The time course of unchanged plasma $^{11}$C-FMZ can be obtained from that of the unchanged plasma $^{123}$I-IMZ using the following relationship: $^{11}$C-FMZ = $(f_{1FMZ}/f_{1IMZ}) \times (^{123}$I-IMZ$/(0.72\ e^{-0.08[t-6.3]}))$. The values used for the free fraction of plasma parent compound, $f_1$, were $f_{1FMZ} = 0.5$ and $f_{1IMZ} = 0.33$ (7,8,33).

### Image Processing

For anatomic localization of the cortical structures, a T1-weighted brain MR image volume was obtained for each volunteer (Eclipse, Picker; 1.5 T; repetition time = 15 ms; echo time = 4 ms; pixel size = 0.98 × 0.98 × 1.10 mm). To realign the MRI to the SPECT images, SPECT frames 23–30 were averaged to produce a mean SPECT image, which provided a satisfactory definition of the whole brain anatomy. For each volunteer, the MR image was aligned with the volunteer's mean SPECT image using Automated Image Registration (version 3.08) software (34,35) with a rigid body transformation (6 parameters) algorithm. The PET images were also realigned with the SPECT images.

### Data Analysis

Using MR images to identify cerebral structures, ROIs (radius = 5 mm) were placed, including the cerebellum, the pons, and the temporal, frontal, and occipital cortices. These ROIs were then applied to the dynamic SPECT images, and the time–concentration curves were extracted.

For comparison of PET and SPECT $B'_{max}$ for the volunteer who underwent both experiments, we used a set of 146 ROIs (radius = 10 mm) placed in the whole brain on MR images and applied them to the dynamic PET and SPECT images. Because of the high noise level in the SPECT data, there were divergences in kinetic parameters in 5 of the 146 ROIs during the identification procedure. These 5 ROIs corresponded to brain regions involving white matter with a very low signal-to-noise ratio and were not used for further analysis. Model parameters were identified through minimization of a weighted least-square cost function using a Marquardt algorithm (36).

## RESULTS

### Identification of Common Parameters

Figure 3 shows an example of a coupled fit for 1 volunteer. All time–concentration curves were correctly fitted by the model shown in Figure 1. The mean values of the
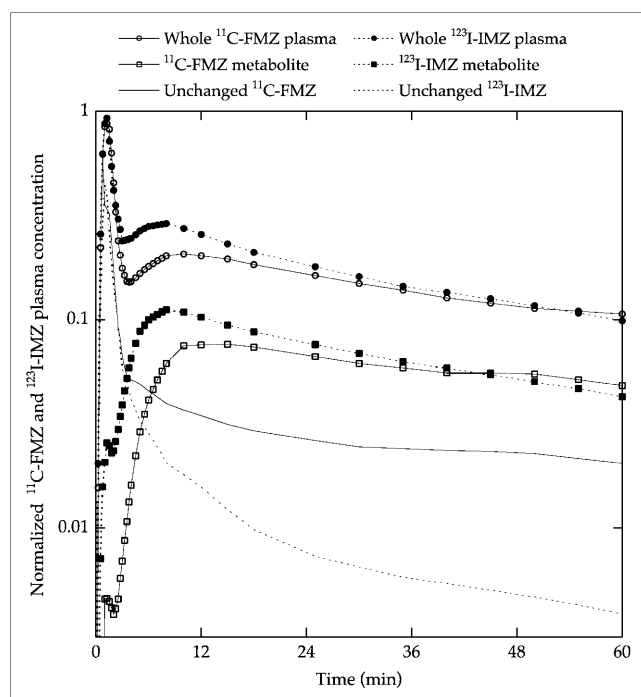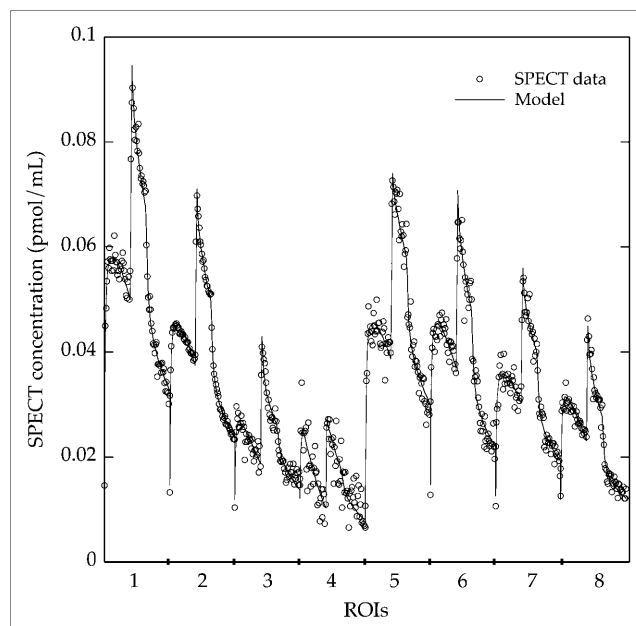


**FIGURE 2.** Time courses of $^{11}$C-FMZ and $^{123}$I-IMZ plasma components obtained from previous study for 7 healthy volunteers (14). Time courses of unchanged plasma levels of both tracers are linked by the following relationship: $^{11}$C-FMZ = $(f_{1FMZ}/f_{1IMZ}) \times (^{123}$I-IMZ$/(0.72\ e^{-0.08[t-6.3]}))$, where $f_{1FMZ} = 0.5$ and $f_{1IMZ} = 0.33$.



**FIGURE 3.** Example with 1 volunteer of a coupled fit obtained among 8 ROIs placed on gray matter (1), whole brain (2), white matter (3), pons (4), occipital cortex (5), frontal cortex (6), temporal cortex (7), and cerebellum (8). Common parameters were estimated simultaneously, and resulting values were used as constants to simplify the model.

common parameters across volunteers were $A = 1.18 \pm 0.36$, $B = 5.74 \pm 2.39$, $C = 1.58 \pm 0.67$, and $D = 5.18 \pm 3.68$. We deduced from A/B that $DV_{f+ns\text{-}FMZ}/DV_{f+ns\text{-}IMZ} = 0.206$ and, from D/C, that $K_{d\text{-}FMZ} = 3.28 \times K_{d\text{-}IMZ}$. Afterward, only the constrained model was used to fit IMZ model parameters using individual A, B, C, and D fixed values.

## SPECT Time–Concentration Curves

Figure 4 shows examples of time–concentration curves obtained with protocols 1 (Fig. 4A) and 2 (Fig. 4B) with a large ROI corresponding to the whole brain. A rapid increase in the concentration of radioligand was observed after each labeled injection. At the time of displacement, a rapid decrease was observed regardless of the protocol
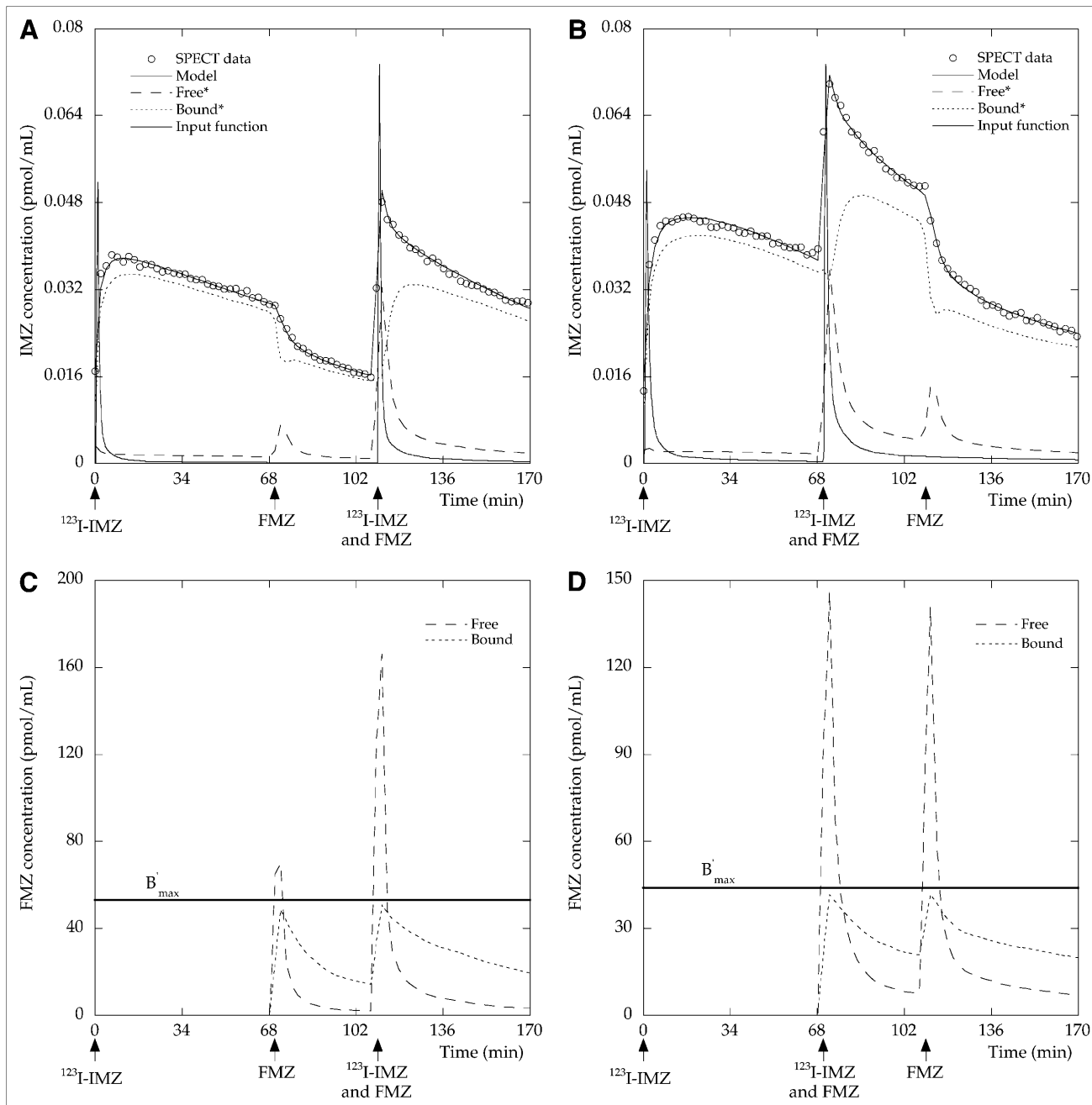


**FIGURE 4.** Compartmental analysis allows simulation of time courses for each compartment: free/nonspecifically bound and specifically bound ligand for $^{123}$I-IMZ (A and B) and FMZ (C and D). The first column corresponds to protocol 1 and the second column corresponds to protocol 2. Only the labeled input function of the model is represented here. Estimated IMZ model parameters were as follows: for A and C, $B'_{max} = 53 \pm 1$ pmol/mL, $K_1 = 0.54 \pm 0.01$ min$^{-1}$, $k'_2 = 0.19 \pm 0.01$ min$^{-1}$, $k_{on}/V_R = 0.071 \pm 0.003$ mL/pmol·min, $k_{off} = 0.18 \pm 0.01$ min$^{-1}$; and for B and D, $B'_{max} = 44 \pm 2$ pmol/mL, $K_1 = 0.44 \pm 0.01$ min$^{-1}$, $k_2 = 0.20 \pm 0.01$ min$^{-1}$, $k_{on}/V_R = 0.100 \pm 0.003$ mL/pmol·min, $k_{off} = 0.24 \pm 0.01$ min$^{-1}$.

used. The injection of FMZ resulted in approximately 30% displacement of $^{123}$I-IMZ.

The time courses of the radioligand concentration in all model compartments can be simulated. We found that the measured SPECT activity corresponded mainly to the specifically bound radioligand (Figs. 4A and 4B). The large dose of unlabeled FMZ injected during displacement causes a large decrease in the labeled ligand, and this effect is more accentuated with protocol 2. Figures 4C and 4D show that a large proportion of the receptors were occupied by the unlabeled ligand when FMZ was injected.

### Estimates of Individual Parameters

Table 2 shows average values of model parameters estimated for 5 ROIs in the 8 volunteers. Because there was no significant difference in the fit obtained by protocols 1 and 2, we averaged all estimated values. The $B'_{max}$ values varied across the regions from 7 to 69 pmol/mL and the $K_dV_R$ values ranged from 2.3 to 3.7 pmol/mL. In addition, the $K_{1\text{-IMZ}}$ values ranged from 0.55 to 0.77 min$^{-1}$, and the $k'_{2\text{-IMZ}}$ values ranged from 0.14 to 0.83 min$^{-1}$. We also calculated high values for $K_{1\text{-FMZ}}$ and $k'_{2\text{-IMZ}}$, ranging from 0.63 to 0.86 and from 0.76 to 5.03, respectively.

We next compared the distribution volume values ($DV_T''$) calculated using 2-compartment model parameters and the first labeled injection with the $DV_T$ values calculated using IMZ parameters estimated from the dual-ligand approach and Equation 6. We obtained a quasilinear relationship with a correlation coefficient close to unity (Fig. 5A). We further compared the $DV_T''$ values with the corresponding $B'_{max}$ values. In spite of some variability, there was an acceptable correlation between these 2 parameters (Fig. 5B).

### Direct Comparison of SPECT and PET

Figure 6 shows a direct comparison between $B'_{max}$ values obtained in the same volunteer using PET and SPECT.

Figure 6 shows a clear relationship between PET and SPECT $B'_{max}$ values.

### DISCUSSION

A full in vivo quantification of brain receptors with PET or SPECT requires multiple injections of labeled or unlabeled ligand to change receptor occupancy. However, the administration of a large dose of unlabeled ligand can produce pharmacologic effects, precluding its use in humans. This problem requires the modification of experimental protocols and the adaptation of a kinetic model. This is the case for IMZ, a partial inverse agonist that binds to benzodiazepine sites producing pharmacologic effects when administered at high doses. By replacing unlabeled IMZ with FMZ, an antagonist with negligible pharmacologic effects, it was possible to use $^{123}$I-IMZ and SPECT to quantify the benzodiazepine receptors.

In this study, we developed a dual-ligand approach to separately estimate the density of benzodiazepine receptors and ligand affinity. We adjusted the model to take into account the different kinetics of the 2 ligands.

### Model Simplifications

IMZ and FMZ have high specificities and affinities for the same type of receptor sites. Time–concentration curves of each ligand can therefore be described by a 2-tissue compartment model including free ligand and specific binding (7–11,14,15,25). The brain distribution of both ligands has been compared in vitro (17) and with many in vivo studies using patients and healthy volunteers (14,37). Similar brain distributions for both ligands have been described after injection of $^{11}$C-FMZ and $^{123}$I-IMZ. Therefore, we have assumed in this study that both ligands compete for the same type of receptor sites and, thus, had the same $B'_{max}$.

### TABLE 2
Mean Model Parameter Values Estimated Using Dual-Ligand Approach Across 8 Subjects

| Parameter ± SD | Cerebellum | Pons | Frontal ctx | Temporal ctx | Occipital ctx |
|---|---|---|---|---|---|
| Fitted | | | Iomazenil | | |
| $B'_{max}$ (pmol/mL) | 42 ± 14 | 7 ± 7 | 39 ± 12 | 40 ± 10 | 69 ± 24 |
| $K_1$ (min$^{-1}$) | 0.70 ± 0.23 | 0.55 ± 0.36 | 0.67 ± 0.24 | 0.56 ± 0.19 | 0.77 ± 0.25 |
| $k'_2$ (min$^{-1}$) | 0.25 ± 0.08 | 0.83 ± 0.79 | 0.19 ± 0.12 | 0.14 ± 0.06 | 0.21 ± 0.14 |
| $k_{on}/V_R$ (mL/pmol·min) | 0.100 ± 0.038 | 0.081 ± 0.102 | 0.083 ± 0.040 | 0.084 ± 0.030 | 0.072 ± 0.035 |
| $k_{off}$ (min$^{-1}$) | 0.20 ± 0.09 | 0.07 ± 0.05 | 0.19 ± 0.12 | 0.20 ± 0.12 | 0.20 ± 0.12 |
| $K_dV_R$ (pmol/mL) | 2.1 ± 0.8 | 2.5 ± 4.2 | 2.4 ± 1.4 | 2.3 ± 0.8 | 3.7 ± 2.9 |
| Calculated* | | | Flumazenil | | |
| $K_1$ (min$^{-1}$) | 0.78 ± 0.23 | 0.63 ± 0.43 | 0.75 ± 0.27 | 0.63 ± 0.23 | 0.86 ± 0.30 |
| $k'_2$ (min$^{-1}$) | 1.38 ± 0.67 | 5.03 ± 5.45 | 1.11 ± 1.11 | 0.76 ± 0.34 | 1.09 ± 0.70 |
| $k_{on}/V_R$ (mL/pmol·min) | 0.146 ± 0.082 | 0.146 ± 0.198 | 0.112 ± 0.043 | 0.118 ± 0.048 | 0.111 ± 0.082 |
| $k_{off}$ (min$^{-1}$) | 0.78 ± 0.29 | 0.24 ± 0.09 | 0.83 ± 0.55 | 0.76 ± 0.30 | 0.79 ± 0.33 |
| $K_dV_R$ (pmol/mL) | 6.2 ± 2.4 | 9.0 ± 15.5 | 7.3 ± 4.1 | 7.1 ± 2.8 | 10.8 ± 9.8 |

*Calculated parameters using fixed A, B, C, and D values.
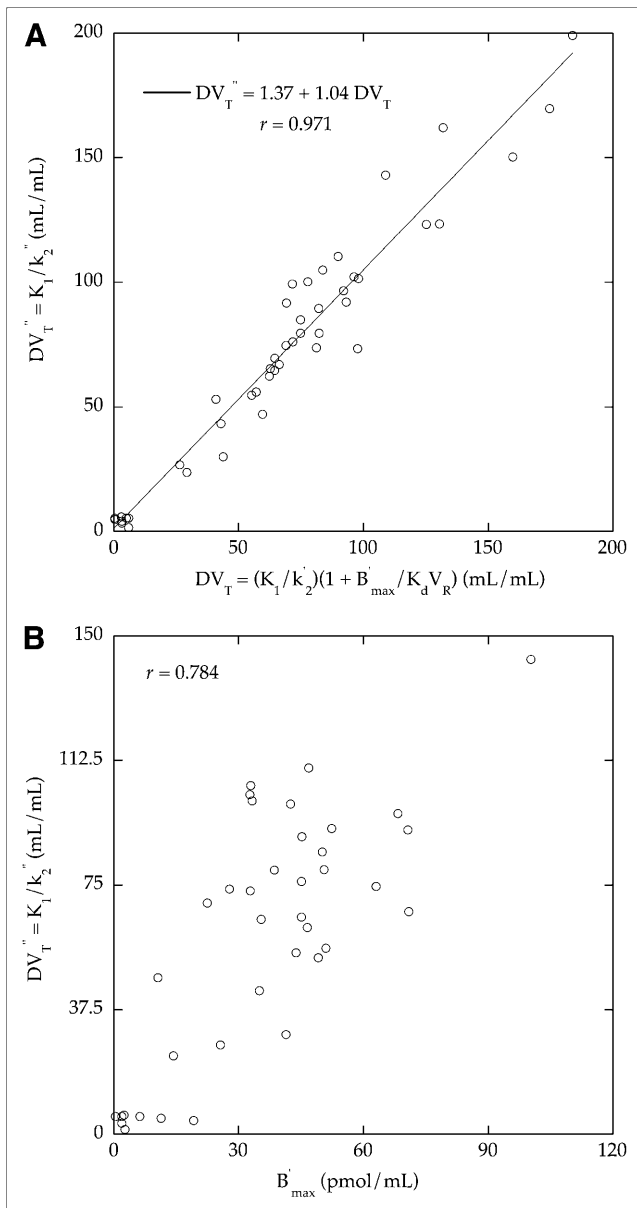ctx = cortex.

FIGURE 5. (A) Comparison across regions and volunteers between distribution volume values estimated using 3-compartment model parameters ($DV_T$) and 2-compartment model parameters ($DV_T''$). Quasiidentity line was obtained between values. (B) Comparison between $B'_{max}$ values and their corresponding $DV_T''$ values estimated with 2-compartment model.

The compartment model adapted for the dual-ligand approach involves 2 distinct parts to describe separately the kinetics of $^{123}$I-IMZ and FMZ. Each part of the model has its own parameters, but the total receptor site concentration available for binding, $B'_{max}$, is common to both ligands. Thus, the resulting compartment model involves 9 unknown parameters. As previously shown in multiinjection PET studies (33,38), only 5 or 6 parameters can be estimated with acceptable SEs. Thus, to avoid identification problems during the fitting procedure, it was necessary to
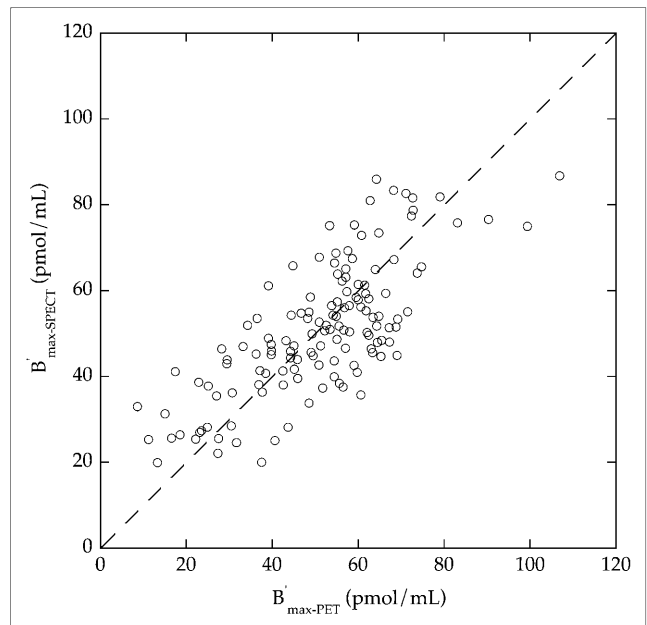


FIGURE 6. Direct comparison between $B'_{max}$ values obtained in same volunteer with PET multiinjection approach and with SPECT dual-ligand approach. Dashed line corresponds to identity line.

simplify the model and reduce the number of parameters. Consequently, we assumed a linear relationship between the kinetic parameters for $^{123}$I-IMZ and FMZ throughout the brain. In this way, we obtained 4 constants, A, B, C, and D, between IMZ and FMZ parameters that could explain this relationship. We first considered that the $DV_{f+ns}$ values were constant and independent of the receptor density. Inhibition studies in gray matter regions have estimated this value to be 0.68 for FMZ and 3.2 for IMZ (8,33,39). Second, we considered constant the $k_{off}$ parameter value because several authors have shown that its value is independent of the receptor density (39,40). Assuming that the BP parameter is a good index of receptor density, as shown in previous IMZ and FMZ studies (14,16), the $(BP_{FMZ}/BP_{IMZ})$ ratio can be considered constant.

These relationships are theoretic, and for each volunteer we adjusted all of the parameters using a coupled fitting procedure. This procedure reduces the number of estimated parameters to 5 and improves the stability of the final fit. The mean $DV_{f+ns-FMZ}/DV_{f+ns-IMZ}$ ratio (0.206) that we obtained across subjects is in agreement with other values in the literature ($DV_{f+ns-FMZ}/DV_{f+ns-IMZ}$ = 0.68/3.2 = 0.2125) (7,8,33). In contrast, the dissociation constant calculated using the D/C ratio was between 10 and 20, which was smaller than that previously reported with in vitro studies (9,25,41). Because our study has been performed in vivo, it is difficult to compare these results.

**Input Functions of Model**

The quantitative approach based on a multiinjection protocol is one of the more complete methods for studying

ligand–receptor interactions. However, this model assumes that each injection of labeled or unlabeled ligand, administered with a same volume, results in similar time–concentration plasma curves proportional to the mass injected (*10*). In this case, the unlabeled input function required to solve the model equations is calculated by simulation using the labeled input function. In our study, we estimated the relationship between $^{123}$I-IMZ and $^{11}$C-FMZ plasma input functions by comparing the time courses of both ligands in a group of volunteers. We found that the IMZ metabolites in plasma rose faster than the FMZ metabolites. After subtraction of the metabolite time course, the time courses for unchanged IMZ and FMZ plasma compounds were very similar, although the fraction of ligand bound to protein ($f_1$) was higher for IMZ. Therefore, using known values for $f_1$ and by applying the relationship between the 2 ligands, it was possible to calculate $C_p(t)$ for FMZ.

## SPECT Time–Concentration Curves and Estimated Values

One of the main interests of the kinetic approach is the possibility to estimate the time course of each compartment. The displacement of $^{123}$I-IMZ by injection of FMZ logically has an effect on the specific binding of $^{123}$I-IMZ, but the effect was weaker than for $^{11}$C-FMZ, where approximately 70% of the labeled molecules were displaced in the occipital cortex with only 0.01 mg/kg of unlabeled FMZ (*10*). There are several possible explanations for this effect, including differences in lipophilicity, affinity, and nonspecific binding between the 2 molecules (*17,25,42*).

The range of receptor density values obtained in our study fits well with previous reports (*10,14,33*). The magnitude of the $k_{on}/V_R$ values for IMZ was close to that obtained for FMZ. As expected, we obtained lower $k_{off}$ values, and thus lower $K_dV_R$ values, for IMZ than for FMZ (*7,8,14,25*).

The high $K_{1\text{-FMZ}}$ values calculated in some volunteers may be due to the use of an incorrect value for the $f_1$ parameter. In the model equations, the $f_1$ parameter is linked with the input function and, hence, with the $K_1$ parameter. Therefore, an erroneously low $f_1$ value would artificially increase the $K_{1\text{-FMZ}}$ parameter. However, a similar increase in $k'_{2\text{-FMZ}}$ was estimated by the model, leading to a compensated value for the distribution volume ($DV_{f+ns\text{-FMZ}}$).

Furthermore, we compared the distribution volume values estimated using the dual-ligand approach ($DV_T$) with those obtained using the data corresponding to the first tracer injection and a 2-compartment model ($DV_T''$). We also directly compared the $DV_T''$ and $B'_{max}$ values. Our results show an identity relationship between the $DV_T$ and $DV_T''$ parameters and a good correlation between $DV_T''$ and $B'_{max}$. These correlations demonstrate that the model is effective at estimating the parameters despite high variability in the SPECT data.

We did not find significant differences when we switched the order of the displacement and coinjection. The goal of protocol 2, in which the displacement was performed after the coinjection, was to accumulate a higher signal at the time of displacement and produce a stronger displacement of labeled ligand. The lack of differences can be explained by the presence of a significant displacement effect already obtained with protocol 1. However, protocol 2 could be more appropriate for studies with low signal-to-noise ratios, which occur when the size of the ROIs for parametric imaging is reduced.

## Direct Comparison of PET and SPECT

Finally, in 1 volunteer, we directly compared the $B'_{max}$ values obtained using the PET multiinjection approach with those obtained using the SPECT dual-ligand approach. Visually, there was a clear correlation between PET and SPECT $B'_{max}$ values. However, noise related to differences between PET and SPECT measurements should be considered. Specifically, the attenuation correction is directly measured in PET but is only corrected by a mathematic model (Chang method) in SPECT. In addition, the partial-volume effects are different for the PET and SPECT data.

## CONCLUSION

This work demonstrates a theoretic framework and initial application in SPECT. We have shown that it is possible to quantify binding parameters with SPECT using an adaptation of the multiinjection approach. This new method, named the dual-ligand approach, enables the quantification of all model parameters with acceptable SEs. Moreover, we showed that unlabeled ligands devoid of pharmacologic effects can expand the number of quantification studies that can be performed using PET and SPECT.

## REFERENCES

1. Ryvlin P, Bouvard S, Le Bars D, et al. Clinical utility of flumazenil-PET versus [$^{18}$F]fluorodeoxyglucose-PET and MRI in refractory partial epilepsy: a prospective study in 100 patients. *Brain.* 1998;121:2067–2081.
2. Savic I, Roland P, Sedvall G, Persson A, Pauli S, Widen L. In-vivo demonstration of reduced benzodiazepine receptor binding in human epileptic foci. *Lancet.* 1988;2:863–866.
3. Verhoeff NP, Soares JC, D'Souza CD, et al. [$^{123}$I]Iomazenil SPECT benzodiazepine receptor imaging in schizophrenia. *Psychiatry Res.* 1999;91:163–173.
4. Pappata S, Samson Y, Chavoix C, Prenant C, Maziere M, Baron JC. Regional specific binding of [$^{11}$C]RO 15 1788 to central type benzodiazepine receptors in human brain: quantitative evaluation by PET. *J Cereb Blood Flow Metab.* 1988;8:304–313.
5. Persson A, Ehrin E, Eriksson L, et al. Imaging of [$^{11}$C]-labelled Ro 15-1788 binding to benzodiazepine receptors in the human brain by positron emission tomography. *J Psychiatr Res.* 1985;19:609–622.

6. Persson A, Pauli S, Halldin C, et al. Saturation analysis of specific [11]C Ro 15-1788 binding to the human neocortex using positron emission tomography. *Hum Psychopharmacol.* 1989;4:21–31.

7. Abi-Dargham A, Gandelman M, Zoghbi SS, et al. Reproducibility of SPECT measurement of benzodiazepine receptors in human brain with iodine-123-iomazenil. *J Nucl Med.* 1995;36:167–175.

8. Abi-Dargham A, Laruelle M, Seibyl J, et al. SPECT measurement of benzodiazepine receptors in human brain with iodine-123-iomazenil: kinetic and equilibrium paradigms. *J Nucl Med.* 1994;35:228–238.

9. Laruelle M, Abi Dargham A, Al Tikriti MS, et al. SPECT quantification of [123]Iiomazenil binding to benzodiazepine receptors in nonhuman primates. II. Equilibrium analysis of constant infusion experiments and correlation with in vitro parameters. *J Cereb Blood Flow Metab.* 1994;14:453–465.

10. Delforge J, Pappata S, Millet P, et al. Quantification of benzodiazepine receptors in human brain using PET, [^{11}C]flumazenil, and a single-experiment protocol. *J Cereb Blood Flow Metab.* 1995;15:284–300.

11. Lassen NA, Bartenstein PA, Lammertsma AA, et al. Benzodiazepine receptor quantification in vivo in humans using [^{11}C]flumazenil and PET: application of the steady-state principle. *J Cereb Blood Flow Metab.* 1995;15:152–165.

12. Lammertsma AA, Lassen NA, Prevett MC, et al. Quantification of benzodiazepine receptors in vivo using ^{11}C-flumazenil: application of the steady state principle. In: Uemura K, Jones T, Lassen NA, Kanno I, eds. *Quantification of Brain Function: Tracer Kinetics and Image Analysis in Brain PET.* Amsterdam, The Netherlands: Elsevier Science; 1993:303–311.

13. Koeppe RA, Holthoff VA, Frey KA, Kilbourn MR, Kuhl DE. Compartmental analysis of [^{11}C]flumazenil kinetics for the estimation of ligand transport rate and receptor distribution using positron emission tomography. *J Cereb Blood Flow Metab.* 1991;11:735–744.

14. Millet P, Graf C, Buck A, et al. Similarity and robustness of PET and SPECT binding parameters for benzodiazepine receptors. *J Cereb Blood Flow Metab.* 2000;20:1587–1603.

15. Laruelle M, Baldwin RM, Rattner Z, et al. SPECT quantification of [123]Iiomazenil binding to benzodiazepine receptors in nonhuman primates. I. Kinetic modeling of single bolus experiments. *J Cereb Blood Flow Metab.* 1994;14:439–452.

16. Millet P, Graf C, Buck A, Walder B, Ibanez V. Evaluation of the reference tissue models for PET and SPECT benzodiazepine binding parameters. *Neuroimage.* 2002;17:928–942.

17. Beer HF, Blauenstein PA, Hasler PH, et al. In vitro and in vivo evaluation of iodine-123-Ro 16-0154: a new imaging agent for SPECT investigations of benzodiazepine receptors. *J Nucl Med.* 1990;31:1007–1014.

18. Darragh A, Lambe R, O'Boyle C, Kenny M, Brick I. Absence of central effects in man of the benzodiazepine antagonist Ro 15-1788. *Psychopharmacology (Berl).* 1983;80:192–195.

19. Kouris K, Clarke GA, Jarritt PH, Townsend CE, Thomas SN. Physical performance evaluation of the Toshiba GCA-9300A triple-headed system. *J Nucl Med.* 1993;34:1778–1789.

20. Mahmood S, Buscombe JR, Kouris K, et al. Clinical experience with a multidetector SPET system (Toshiba GCA-9300A). *Nucl Med Commun.* 1994;15:643–652.

21. Ogawa K. Simulation study of triple-energy-window scatter correction in combined Tl-201, Tc-99m SPECT. *Ann Nucl Med.* 1994;8:277–281.

22. Hayashi M, Deguchi J, Utsunomiya K, et al. Comparison of methods of attenuation and scatter correction in brain perfusion SPECT. *J Nucl Med Technol.* 2005;33:224–229.

23. Barre L, Debruyne D, Abadie P, Moulin M, Baron JC. A comparison of methods for the separation of [^{11}C]Ro 15-1788 (flumazenil) from its metabolites in the blood of rabbits, baboons and humans. *Int J Rad Appl Instrum [A].* 1991;42:435–439.

24. Debruyne D, Abadie P, Barre F, et al. Plasma pharmacokinetics and metabolism of the benzodiazepine antagonist [^{11}C]Ro 15-1788 (flumazenil) in baboon and human during positron emission tomography studies. *Eur J Drug Metab Pharmacokinet.* 1991;16:141–152.

25. Westera G, Buck A, Burger C, Leenders KL, von Schulthess GK, Schubiger AP. Carbon-11 and iodine-123 labelled iomazenil: a direct PET-SPET comparison. *Eur J Nucl Med.* 1996;23:5–12.

26. Delforge J, Syrota A, Bendriem B. Concept of reaction volume in the in vivo ligand-receptor model. *J Nucl Med.* 1996;37:118–125.

27. Farde L, Eriksson L, Blomquist G, Halldin C. Kinetic analysis of central [^{11}C]raclopride binding to D-2-dopamine receptors studied by PET: a comparison to the equilibrium analysis. *J Cereb Blood Flow Metab.* 1989;9:696–708.

28. Perlmutter JS, Larson KB, Raichle ME, et al. Strategies for in vivo measurement of receptor binding using positron emission tomography. *J Cereb Blood Flow Metab.* 1986;6:154–169.

29. Renkin EM. Transport of potassium-42 from blood to tissue in isolated mammalian skeletal muscles. *Am J Physiol.* 1959;197:1205–1210.

30. Huesman RH, Coxson PG. Consolidation of common parameters from multiple fits in dynamic PET data analysis. *IEEE Trans Med Imaging.* 1997;16:675–683.

31. Sanabria-Bohorquez SM, Labar D, Leveque P, et al. [^{11}C]Flumazenil metabolite measurement in plasma is not necessary for accurate brain benzodiazepine receptor quantification. *Eur J Nucl Med.* 2000;27:1674–1683.

32. Delforge J, Syrota A, Mazoyer BM. Identifiability analysis and parameter identification of an in vivo ligand-receptor model from PET data. *IEEE Trans Biomed Eng.* 1990;37:653–661.

33. Price JC, Mayberg HS, Dannals RF, et al. Measurement of benzodiazepine receptor number and affinity in humans using tracer kinetic modeling, positron emission tomography, and [^{11}C]flumazenil. *J Cereb Blood Flow Metab.* 1993;13:656–667.

34. Woods RP, Cherry SR, Mazziotta JC. Rapid automated algorithm for aligning and reslicing PET images. *J Comput Assist Tomogr.* 1992;16:620–633.

35. Woods RP, Mazziotta JC, Cherry SR. MRI-PET registration with automated algorithm. *J Comput Assist Tomogr.* 1993;17:536–543.

36. Marquardt DW. An algorithm for least squares estimation of non-linear parameters. *J Soc Indian Appl Math.* 1963;2:431–441.

37. Ohyama M, Senda M, Ishiwata K, et al. Preserved benzodiazepine receptors in Alzheimer's disease measured with C-11 flumazenil PET and I-123 iomazenil SPECT in comparison with CBF. *Ann Nucl Med.* 1999;13:309–315.

38. Delforge J, Syrota A, Bottlaender M, et al. Modeling analysis of [^{11}C]flumazenil kinetics studied by PET: application to a critical study of the equilibrium approaches. *J Cereb Blood Flow Metab.* 1993;13:454–468.

39. Millet P, Delforge J, Mauguiere F, et al. Parameter and index images of benzodiazepine receptor concentration in the brain. *J Nucl Med.* 1995;36:1462–1471.

40. Ginovart N, Wilson AA, Meyer JH, Hussey D, Houle S. Positron emission tomography quantification of [^{11}C]-DASB binding to the human serotonin transporter: modeling strategies. *J Cereb Blood Flow Metab.* 2001;21:1342–1353.

41. Johnson EW, Woods SW, Zoghbi S, McBride BJ, Baldwin RM, Innis RB. Receptor binding characterization of the benzodiazepine radioligand ^{125}I-Ro16-0154: potential probe for SPECT brain imaging. *Life Sci.* 1990;47:1535–1546.

42. Zoghbi SS, Baldwin RM, Seibyl JP, et al. Pharmacokinetics of the SPECT benzodiazepine receptor radioligand [123]Iiomazenil in human and non-human primates. *Int J Rad Appl Instrum B.* 1992;19:881–888.